



Fracture mechanics investigation on brittle fracture behavior under cyclic load in steel beam-end connections with proportional shapes

T. Kawabata(1), T. Nakagomi(2), S. Kishiki(3), S. Aoyagi(4), Y. Murata(5), K. Kasai(6)

(1) Professor, The University of Tokyo, kawabata@fract.t.u-tokyo.ac.jp

(2) Professor Emeritus, Shinshu University, nakagom@shinshu-u.ac.jp

(3) Associate Professor, Tokyo Institute of Technology, kishiki.s.aa@m.titech.ac.jp

(4) Former Graduate student, Tokyo Institute of Technology, aoyagi.hs9.satoshi@jp.nipponsteel.com

(5) Graduate student, Shinshu University, 18w5029c@shinshu-u.ac.jp

(6) Special Appointed Professor, Tokyo Institute of Technology, kasai.k.ac@m.titech.ac.jp

...

Abstract

Three sizes tests using beam-column connection models (with and without artificial defects), which are designed and manufactured so as to have almost the proportional dimensional ratio, were carried out under cyclic loading with progressively increasing moment amplitude in winter season temperature environment. In every specimens, the load capacity was completely lost by brittle fracture after the significant ductile crack extension in flange member of beam-end portion. As for the specimens with proportionally designed artificial defects, which are introduced at fusion line position, the number of loading cycles markedly decreased as the size of the specimens increased. This is a result of reflecting that the increase in defect size directly increased the fracture driving force. However, in case of the specimen without defect, although larger ductile crack was formed at the time of brittle fracture initiation in larger test specimen, the fractured cycles were almost the same with regardless of the sizes.

To quantitatively understand these contrasting results for the series without artificial defect, two analyzes based on fracture mechanics were performed. In the analyses, we used the critical conditions of brittle fracture initiation for the tested material separately evaluated by the small-scale specimens, which are scale-independent, i.e., Charpy impact specimens and circumferentially notched round-bar specimens. As a result, it is clearly revealed that the critical condition of brittle crack initiation is much different material by material. It will be important in the following discussion that the material of the L size specimen has the highest toughness as shown in Table 1. In order to evaluate the experimental results with normalizing these randomly different toughness properties of materials, we applied two types of analysis. As one analysis, simplified investigation using stress intensity factor was carried out. Another is a detailed evaluation using local mechanical quantities obtained by 3D elasto-plastic FEM. As a result, with combining the results from both approaches, it has shown that larger size specimens are more susceptible to brittle failure due to the increase of ductile crack extension amount and probability of brittle crack initiation. The enlargement of ductile crack extension is presumed to be due to both the effect of increasing the crack tip constraint and the effect of increasing the high strain region by the increase of thickness of the web member. Moreover, it was estimated that the increase of the probability of brittle crack initiation was due to the increase of the fracture potential volume.

Keywords: Steel beam-column joint; Ductile crack extension; Brittle fracture; Constraint effect; Volume effect



1. Introduction

In building structures, which are generally consist of carbon steel in terms of often economical viewpoint, brittle fracture should be considered first as ultimate failure mode that determines the energy absorption potential against the earthquake. Brittle fractures must be avoided because they directly cause instantaneous loss of function of the component. However, brittle fracture has not been a major problem in the field until now because local buckling occurs earlier than fracture because members were made of relatively thin material. However, as the height and size of the layers are increasing recently, the thicknesses of the members used are also increasing, brittle fracture becomes more likely to occur [1]. Brittle fracture exists in other steel structures, such as pressure vessels and ships. In order to evaluate the anti-fracture performance, it is most straightforward to try to test the real structure, but in practice it is difficult in most cases and the performance must be evaluated with a reduced test piece. In the pressure vessel and ship fields, after WWII, fracture mechanics, that is now one academic area, was founded to meet such needs, and standard systems that can be evaluated using reduced test specimens has already been established [2][3]. In recent years, it has been pointed out that these existing evaluation methods are too conservative, and research to improve the evaluation accuracy [4] and standards for correcting the over-conservatism are establishing [5]. However, the structural design and construction of steel buildings is more complicated than pressure vessels and ships, and in Japan, from the viewpoint of economic efficiency, the deformation allowed in design is much larger than in other fields, and it allows the large amount of macroscopic plastic deformation [6]. In a general beam-to-column joint, it is known that even if there is a small defect in the welded portion, it is broken at another weak point, that is, the base material at the bottom of the scallop in the beam. For this reason, when conducting an evaluation test, it is often not assumed that a defect exists in the welded portion. From such a background, fracture mechanics for fatigue crack propagation and fracture from the crack tip, which is generally applied in other field, cannot be used directly. The authors are working to solve these problems including scale effects (dimensional effects) on steel structures in building.

In this study, a comparison test of the energy absorption potential during an earthquake was performed using a full-scale test specimen simulating an actual structure and a test specimen that was reduced stepwise almost in an equal ratio, and the difference of the properties was directly evaluated. Furthermore, Authors try to interpret the results and quantify the mechanism. In this report, using the experimental results shown in the previous report in detail [7], the interpretation of the essence of the scale effect and quantification of the mechanism using the finite element method and/or fracture mechanics are shown.

2. Experimental results and fracture surface observation

2.1 Experimental results

Table 1 shows the dimensions of the specimens to be discussed in this paper quoted from the overall experimental results [7]. As shown in Fig. 1, the test specimen is roughly scaled in three stages of 1: 1/2: 1/4 based on the welded H-shaped cross section BH-1200×500×25×40, span 5500mm (hereinafter referred to as L size, M size, and S size, respectively). In addition, the second specimen of each size includes an artificial defect having a proportional size, which was located at the fusion line position of the welded portion between the column and the beam flange (Fig. 2). The experiment was conducted with a three-point bending method, and a column with an H-shaped section was placed in the center.

Table 1 – Configuration of specimens tested

Specimen size	mark	L [mm]	Welding defect dimension [mm]	
			length	depth
BH-300x125x6x12	S N	1375	N/A	
	S WD1		20	4.8
BH-600x250x12x22	M N	2750	N/A	
	M WD2		36.7	8.9
BH-1200x500x25x40	L N	5500	N/A	
	L WD2		66.7	16.2

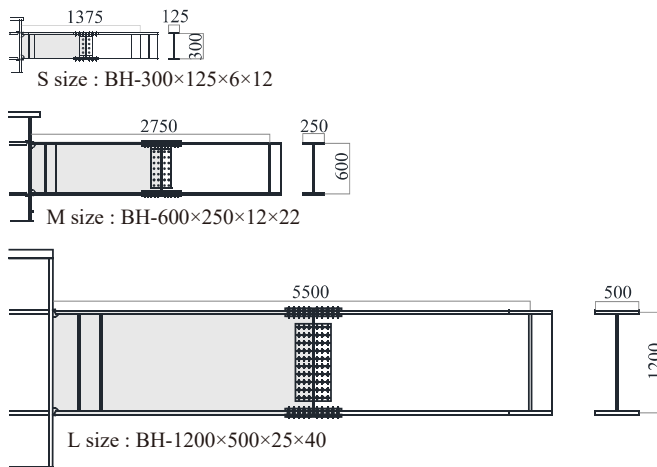


Fig. 1 – Comparison of size of each specimen [7]

The inner span of the beam specimen was 5500 mm for L size, 2750 mm for M size, 1375 mm for S size, and the shear span ratio are designed to be equivalent for all sizes. The loading history is based on the elastic member angle θ_p corresponding to the total plastic moment, and is a cyclic loading with incremental displacement $2\theta_p$ [8].

For evaluation of plastic deformation capability, conventional equivalent cumulative plastic deformation which is calculated by Eq. (1) is used (Fig. 3).

$$E\eta_s = \frac{W_s^+ + W_s^-}{bM_p \cdot b\theta_p} \quad (1)$$

Where, W_s^+ and W_s^- : Energy absorption amount in skelton non-dimensional $M-\theta$ curve (Fig. 3), bM_p : Moment in beam which exhibit plastic deformation attain all section. $b\theta_p$: Deflection angle in beam which exhibit plastic deformation attain all section.

Fig. 4 shows the summary of test results. Only small difference of plastic deformation capability among three-size-specimen without artificial defects is shown, whilst very clear difference exhibits in specimen including defects. This contrast is supposed to come from the microstructure in trigger portion of brittle fracture. In case of a specimen with artificial defects, microstructure of the origin of brittle fracture is almost same in every specimen, because defect is installed in heat affected zone where microstructure is reconstructed by welding thermal history

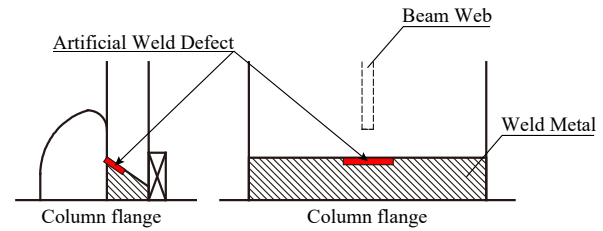


Fig. 2 – Installation position of artificial defect

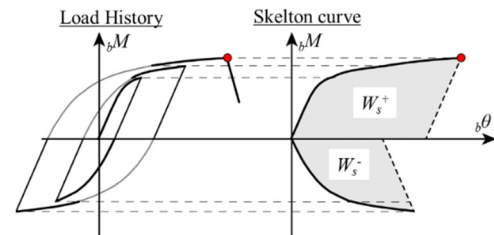


Fig. 3 – Schematic illustration for creation of skeleton curve from experimental raw data

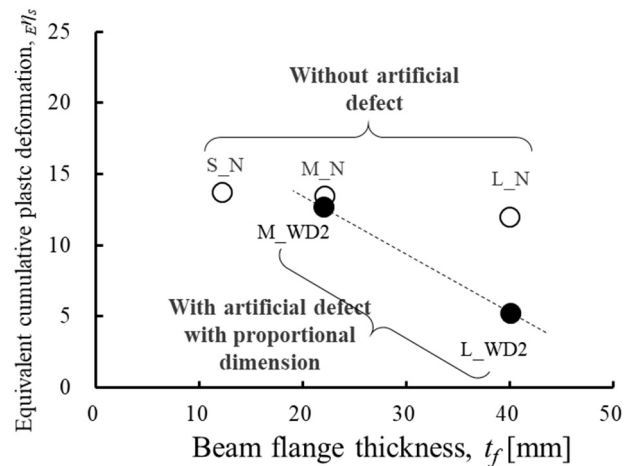


Fig. 4 – Evaluation of experimental results by conventional energy absorption method.

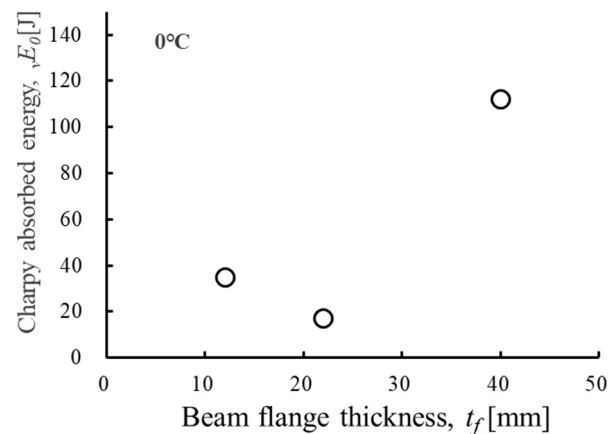


Fig. 5 – Comparison of Charpy impact property



controlled to be almost same in this time fabrication. On the other hand, brittle fracture of a specimen without defect occurs at the root of scallop, that is base plate of beam flange. So the brittle fracture property of structure is directly controlled by toughness of the base plate. Fig. 5 shows the comparison of the Charpy impact value at ambient temperature of base plate of beam flange in each specimen. Although toughness level of the plates was intentionally lowered, difference of the toughness among the material cannot be ignored. This disunity is blocking the fair evaluation regarding to the size of the structure. In this paper, clarification of this is to be investigated.

2.2 Observation of fracture appearance and estimation of fracture morphology

For the interpretation of the fracture test results, observation of fracture surface is always essential. Fig. 6 shows fracture appearance of the specimens including the SEM observation around the trigger position of brittle crack initiation. According to these observations, it was found that the order of fracture was always “ductile fracture initiation, ductile fracture extension, brittle fracture initiation - propagation”. Here, authors thought it is important that the scale effect on building structure is separately considered into ductile fracture and brittle fracture so in the following sections, the scale effect is discussed in the order of fracture, ductile fracture, and brittle fracture. In addition, ductile crack extension was confirmed at the rest three positions of the scallop root, which did not eventually lead to brittle fracture.

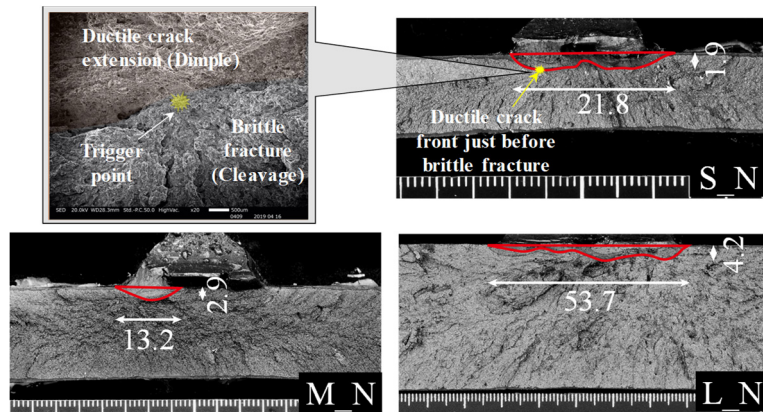


Fig. 6 – Fracture appearance and SEM observation for brittle fracture initiation site (mark S N)

3. Clarification of scale effect on ductile fracture property by local criterion

3.1 Ductile crack initiation and extension measurement by novel constant measurement system

This section discusses the scale effect on ductile crack initiation and propagation in beam-column joints. Generally, it is extremely difficult to identify the ductile fracture occurrence timing by structural experiment. From the fracture surface observation after complete fracture, only the final stage of ductile crack propagation at the time of brittle fracture occurrence was observed, the change in overall rigidity due to the occurrence of ductile crack was very small, and the occurrence timing could not be identified from the load cell signal. In this study, as shown in Fig. 7 small and inexpensive WEB cameras were attached to each of four scallop roots where ductile crack could occur, and the progress of ductile cracks was constantly monitored. Since the ductile crack appeared to occur from the end of unwelded zone in the beam BH welding, it was possible to record the occurrence of ductile crack and the amount of propagation. Fig. 8 summarizes the ductile crack length in the final state in each cycle. It can be inferred that ductile cracks are more likely to be generated and propagated when the specimen is larger. However, since this behavior might changes due to the ductile crack

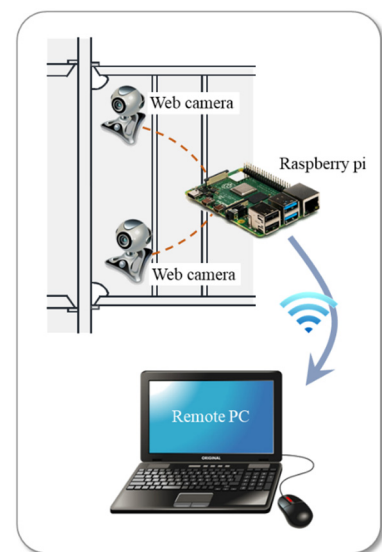


Fig. 7 – Constant observation system by web camera and its communication by Wi-Fi



initiation and propagation properties that are unique to material-by-material, it is necessary to cancel the influence of the material properties in order to discuss only the scale effect precisely.

3.2 Determination of critical conditions of ductile crack initiation and extension property

The ductile crack initiation and extension properties may use fracture mechanics parameters such as J and $CTOD$ [9]. However, in this study, local critical conditions were used, because they are compatible with the finite element method and advantageous for decomposing and studying the scale effect mechanism into various factors. Among various local critical conditions for ductile fracture of metallic materials proposed so far [9], simple and basic equivalent plastic strain criterion was used [10].

For the determination of the critical value, the CTOD test results, which is part of the material test conducted separately from this structural test, were used. The CTOD test was performed in accordance with the method according to ISO12135. Fig. 9 shows the load (P) - clip gauge displacement (V_g) curve of the CTOD test conducted at 10 °C using the beam flange material of the L specimen (hereinafter simply referred to as L material). Brittle fracture did not occur during loading, and ductile fracture always progressed. Fig. 9 also includes the results of the conventional three-dimensional elasto-plastic finite element method. In this method, the fracture phenomenon is not expressed, and it can be seen that the dissociation becomes significant as the ductile crack growth becomes remarkable in the experiment. Here, the finite element method calculation using the element deletion method using the critical strain described above as a criterion was performed. Deleting an element means that the stiffness changes instantaneously and the implicit method makes it difficult to continue the calculation due to instability. Here, a ductile crack

simulation using a dynamic explicit method was performed following the previous study [10]. Table 2 summarizes the calculation conditions. Since the explicit method determines the time increment to satisfy the CFL condition [11], if it is applied to a quasi-static analysis like the subject of this analysis, the calculation time is often too long to be executable. Therefore, it is common to perform mass scaling in which the mass of the target material is set to be larger than the actual value so that the CFL condition is relaxed. Here, the mass was appropriately increased so that the minimum time increment was controlled to about 1×10^{-6} sec. Fig. 10 shows the comparison between experiments and FEM results after optimization of critical equivalent plastic strain. It has to be emphasized that this critical condition is strongly depending on mesh size. This time, crack tip element to be deleted was arranged to $40\mu\text{m}$. As a result, it was found that the critical strain increased in the order of S, M and L, that is, the material L had the highest ductile crack initiation and propagation resistance.

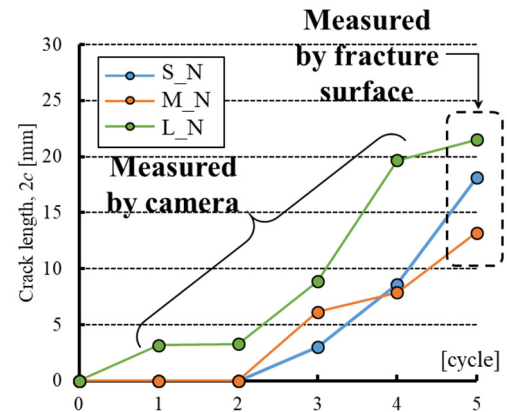


Fig. 8 – Ductile crack initiation and propagation behavior by actual measurement

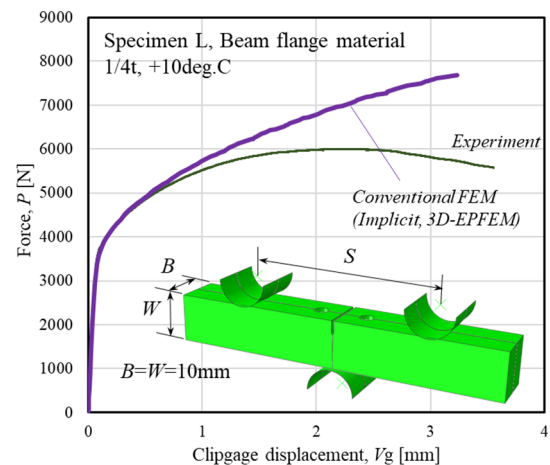


Fig. 9 – CTOD test result that exhibit ductile fracture (material L.)

Table 2 – Calculation conditions for finite element method

Code	Dassault Systèmes, Abaqus 2018
Formulation	Dynamic, explicit
Mass scaling factor	Adjust to minimum time increment= 1×10^{-6} sec.
Loading amplitude	Smooth step



Recall that the ductile crack extension record in the experiments showed that the larger the specimen, the more easily the ductile crack propagated, as shown in Figs. 6 and 8. Here, it was revealed that the larger the specimen, the greater the driving force for ductile crack initiation and propagation, when considered in conjunction with the clarified critical properties of the material.

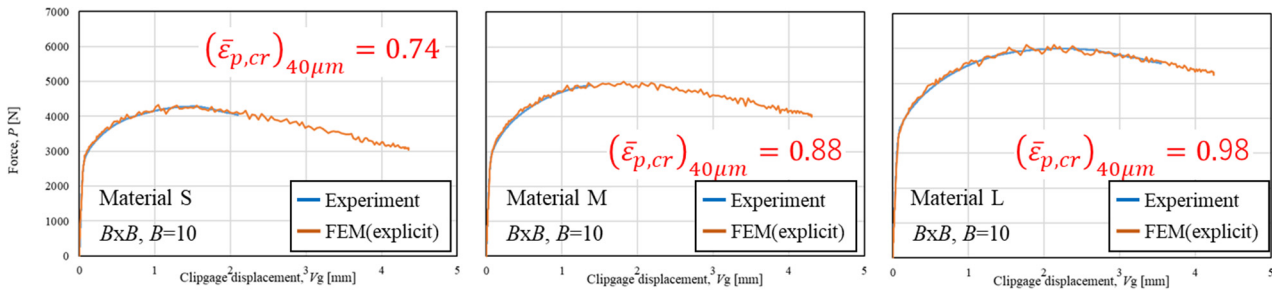


Fig. 10 – Determination of critical strain by optimization of FEM analysis with special element to be deleted

4. Study for scale effect on brittle crack initiation property

4.1 Stochastic study by simplified LEFM

Here, a study using the stress intensity factor (SIF) is performed referring to the previous research [12]. Basically, the SIF for elastoplastic materials should be used only for the deformation scale below the small-scale yield condition [13], but here, it is assumed that SIF concept can be expanded to this problem with large plastic deformation. At the time of the initiation of brittle fracture, it is considered that the SIF as the driving force and the SIF as the critical condition of the material are balanced. The discussion will proceed on both sides.

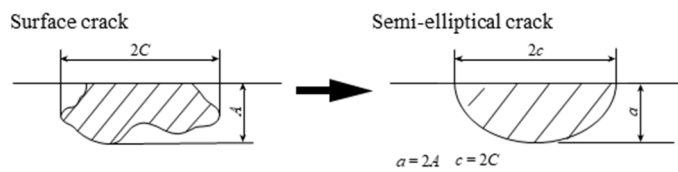


Fig. 11 – Simplification of shape of surface crack

Table 3 – Crack dimension simplification for LEFM study

mark	Thickness, B [mm]	Crack length, 2c [mm]	Crack depth, a [mm]	crack characteristic dimension, \bar{c} [mm]
S N	12	21.8	2.3	2.83
M N	22	13.2	2.9	2.57
L N	40	53.7	3.6	4.40

First, the ductile crack length, which is the source of the driving force required for brittle crack initiation, is obtained from the fracture surface information after the final fracture shown in Fig. 6. At first, since the ductile crack shape has an arbitrary shape crack shape was simplified. After simplifying it to a semi-elliptical shape according to the idea of the fitness-for-service standard (Fig. 11) [2] [3], the SIF at deepest point was calculated according to the handbook value provided by Newman et al [14]. Then a crack characteristic dimension [3] was calculated from the SIF assuming the shape is regarded as the most common shape, infinite plate with through thickness crack. Table 3 shows the crack characteristic dimensions of ductile cracks in each specimen when brittle fracture occurred. The load stress required for the driving force calculation was assumed to be the tensile strength of the material in consideration of the situation where the material was sufficiently plastically deformed.

Next, the conversion formula (Eq. 2) [15] from the Charpy impact energy into critical SIF (K_C) is used for the

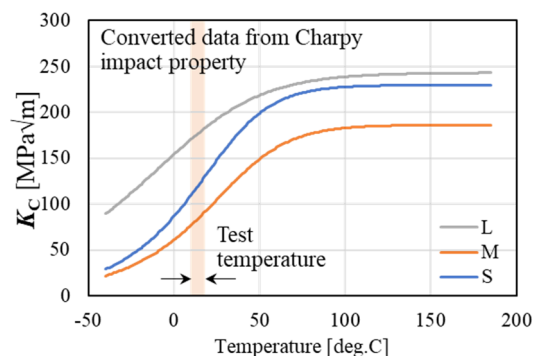


Fig. 12 – Temperature dependency of K_C



critical value. The converted value (at test temperature) is regarded as the critical condition of the material. Since the Charpy impact test is performed on test pieces of the same size irrespective of size, it can be considered as a local value excluding the effect of size and volume (Fig. 12).

$$K_c(\text{MPa}\sqrt{\text{m}}) = 14.6vE(J)^{0.5} \tag{2}$$

However, it is widely known that brittle fracture is not a phenomenon that can be given deterministically but is essentially a stochastic one. This is because the phenomenon is based on the weakest link mechanism [16]. In General, it is assumed that the distribution of the property follows a two-parameter Weibull distribution, and that the distribution has a shape whose shape parameter is assumed to be 4 from the SIF value dominant stress field [17]. Fig. 13 shows the probability density function of K_c for each material. Therefore, an expected value of the Weibull distribution corresponds to the average value shown in Fig. 12. For example, when there was a failure event when the driving force was 200 MPa $\sqrt{\text{m}}$ in material L, the shaded area in the figure indicates the likelihood of this event occurring, in this case about 70%.

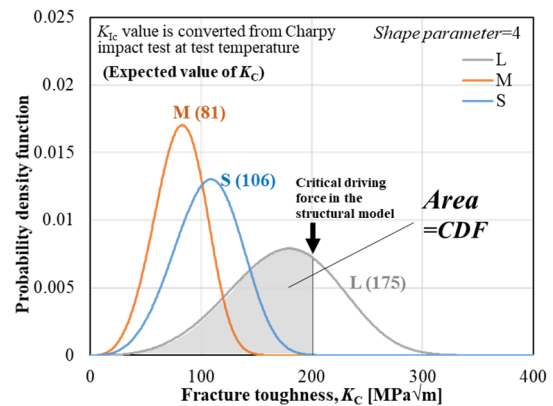


Fig. 13 – Two-parameter Weibull distribution function for toughness of each material

Fig. 14 shows a diagram that considers both the driving force and the critical value distribution discussed so far. In the upper part, the SIF as the driving force for each cycle was calculated, and in the lower part, the driving force value was compared with a critical value distribution to determine the cumulative probability that the phenomenon could occur. Here, since the ductile crack depth during loading could not be determined by camera photographing, it was determined on the assumption that the ductile crack aspect ratio at the time of fracture remained constant. Considering that the structural specimen has a sufficient process zone comparing with the Charpy small specimen, it is considered that the magnitude of the cumulative fracture probability indicates the probability that the phenomenon can occur as a structural specimen. Based on this idea, it is possible to estimate the fracture timing when the same material is virtually used for each specimen. Fig. 15 shows the results. A clear scale effect is observed. However, it would be necessary to study why such a scale effect can be seen while putting various hypotheses in the future.

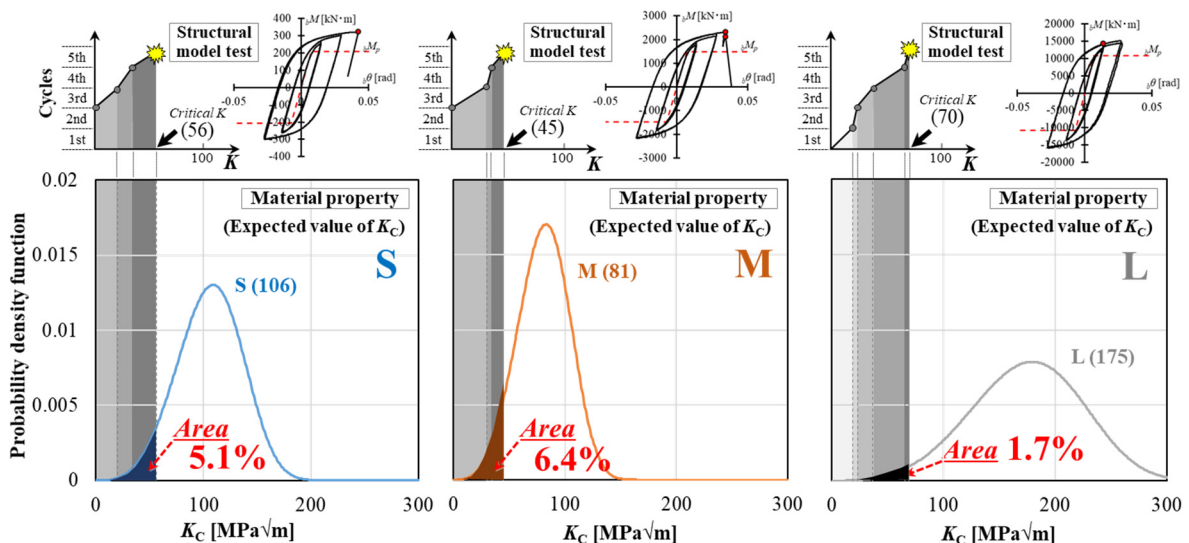


Fig. 14 – Comparison of likelihood for brittle fracture event in each structural size specimen

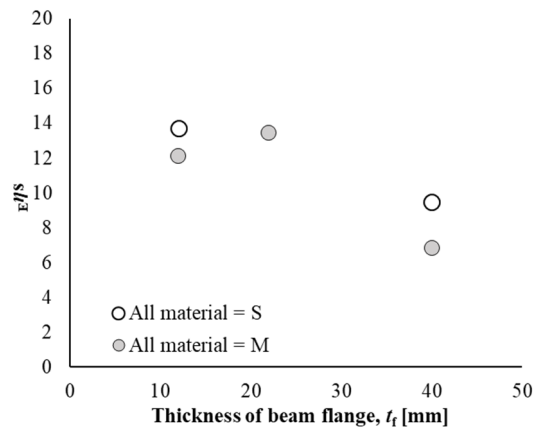


Fig. 15 – Scale effect by normalized equivalent cumulative plastic deformation

4.2 Applicability of critical distance and local critical stress criterion

The concept of characteristic distance stress [16] is based on a stochastic one based on the weakest link mechanism. Here, the characteristic distance is considered the distance from the peak point of the maximum principal stress to the crack tip, so it can be thought that the peak point of the maximum principal stress is a parameter that governs the brittle fracture of a structure or material. Here also, as in the previous section, the critical value of the material is obtained with a small test piece, and the driving force applied to the structure in the fracture cycle is obtained by the three-dimensional elasto-plastic finite element method. In the finite element method, simplified method is used, such that a ductile crack that can be confirmed on the fracture surface after fracture was assumed located from the beginning of the simulation.

The critical value was determined by fracture experiments conducted at -196°C using a round bar specimen with a sharp circumferential notch as shown in Fig. 16 and in parallel with a FEM analysis (two-dimensional axisymmetric element Using). The mesh division is set to $50\ \mu\text{m}$ near the fracture occurrence part at the notch bottom. Fig. 17 shows the FE-model regarding to structural model, which are used for calculating the driving force. Fig. 18 shows the comparison between the increase curve of the peak value of maximum principal stress $(\sigma_1)_{\text{max}}$ as the driving force and the critical maximum principal stress value $(\sigma_1)_{\text{cr}}$ for each material. When the loading step for the actual brittle fracture event, the driving force and the critical value are almost the same. Thus, the brittle fracture behavior of this specimen, that is, the brittle fracture occurrence event in the ductile-brittle transition phenomenon, can be explained by the fracture mechanics approach. In addition, the L specimen shows a slightly lower value of $(\sigma_1)_{\text{max}}$, but it may approach by increasing the number of repetitions of the small material test.

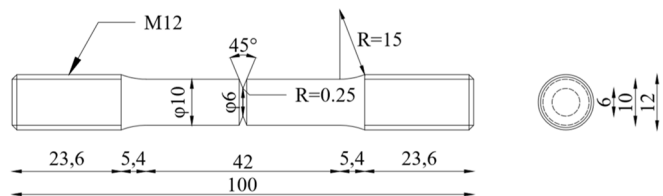


Fig. 16 Circumferentially notched round-bar specimen for obtaining critical stress

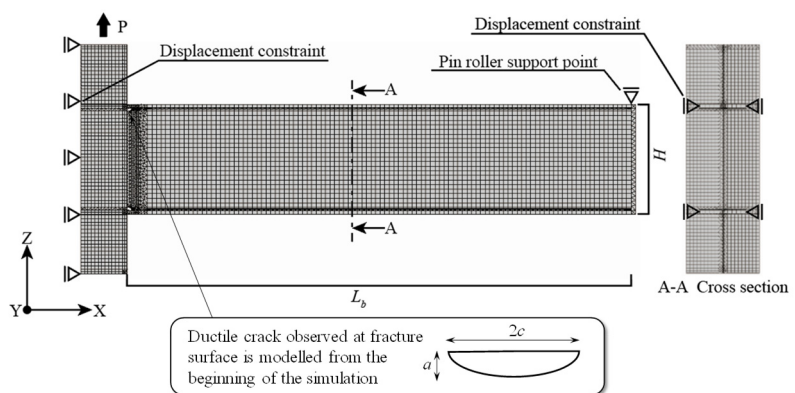


Fig. 17 – general of FE-model for structural model specimen

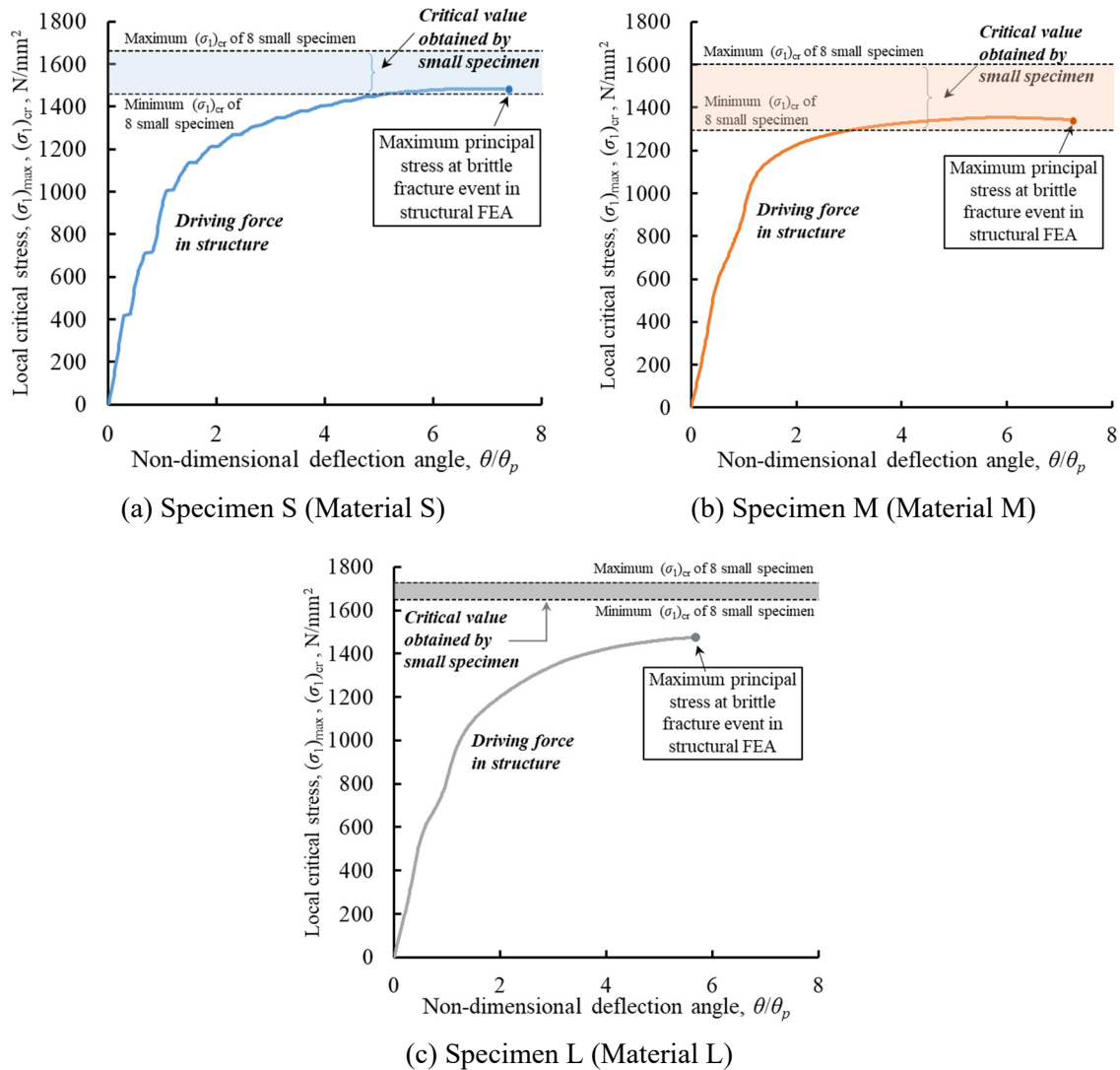


Fig. 18 – Correspondence of the local critical stress obtained by small specimen and driving force at ductile crack tip in structural model

5. Conclusion

To evaluate the applicability of reduced test specimens in evaluating the column-beam joint's holding energy absorption performance during an earthquake, structural experiments were carried out using the specimens which have proportional dimensions almost equal to 1/2 times and 1/4 times based on actual size specimens. In each case, the ductile crack advanced first and the test was terminated by brittle fracture. When the holding performance up to the fracture was organized using the evaluation index with normalized dimensions, there was a problem that the holding performance and the difference of the material toughness were not sufficiently separated, so the scale effect remained unclear. This study re-examines the scale effect by giving some additional considerations to the results. The main results obtained are as follows.

- 1) The scale effect on the driving force for ductile crack growth was clarified by quantifying the local critical strain of each material. The larger the specimen, the earlier the ductile crack is generated and propagated.



- 2) It was clarified through the probabilistic treatment of the brittle fracture resistance of the material that the scale effect was seen on the driving force of brittle fracture.
- 3) Quantification of the scale effect taking into account both of these effects revealed that the 1/4 size specimen had twice the holding performance as the full size specimen. .

However, there are various assumptions in these studies, and the mechanism of the scale effect is not mentioned in this paper. These need to be clarified in the future.

6. Acknowledgements

This research was conducted using the fund of Advanced Loading and Real-scale Experimental Mechanics Laboratory (ALREM) supported by KYB, SWCC Showa Cable Systems Co., Ltd., Japan Iron and Steel Federation, Bridgestone, and OILES Corporation. ALREM belongs to Tokyo Institute of Technology, and is directed by Prof. Kazuhiko Kasai. Invaluable advice was given by the members of the ALREM research committee headed by Prof. Akira Wada.

7. References

- [1] Society of Steel Construction of Japan, The South Hyogo prefecture Earthquake Steel Structure Damage Report, *JSSC Technical report*, 1997.2
- [2] British Standard, *BS 7910:2019*, Guide to methods for assessing the acceptability of flaws in metallic structures, 2019.
- [3] The Japan Welding Engineering Society, *WES2805-2011*, Method of Assessment for Flaws in Fusion Welded Joints with Respect to Brittle Fracture and Fatigue Crack Growth, 2011.
- [4] Beremin F M, Pineau A, Mudry F, Devaux J-C, D'Escatha Y, and Ledermann P (1983), *Metallurgical Transactions A*, Volume 14, pages2277–2287(1983). <https://doi.org/10.1007/BF02663302>.
- [5] International Standard Organization, *ISO 27306:2016*, Method of constraint loss correction of CTOD fracture toughness for fracture assessment of steel components, 2016.
- [6] Itabashi M, Fukuda H, The Japanese Building Standard Law and a series of steels for earthquake-resistant building structures, *Technology, Law and Insurance*, Volume 4, 1999 - Issue 1-2, Pages 37-44.
- [7] Kishiki S, Kawabata T, Nakagomi T, Murata T, Aoyagi S, Kasai K, Experimental Evaluation of Scale Effect on Plastic Deformation Capacity of Steel Beam-End Connection, *17th World Conference on Earthquake Engineering, 17WCEE*, submitting.
- [8] Building Research Institute (2002), The Japan Iron and Steel Federation, Study on Structural Performance Evaluation Test Method for Steel Structures, *Internal Report of Committee*.
- [9] Besson J (2010), Continuum models of ductile fracture : A review. *International Journal of Damage Mechanics*, *SAGE Publications*, 2010, 19, pp.3-52.
- [10] Kawabata T, Ohata M, Minami F (2007), Critical Condition of Ductile Crack Extension and Its Critical Condition of Subsequent Brittle Fracture for High Strength Steel, *Journal of the Japan Society of Naval Architects and Ocean Engineers*, 2007, Volume 5, Pages 235-243.
- [11] https://en.wikipedia.org/wiki/Courant%E2%80%93Friedrichs%E2%80%93Lewy_condition
- [12] Nakagomi T, Hattori K, Ichikawa Y, Matoba K, Iwata M (2002), Experimental Study on Deformation Capacity of Welded Beam-to-Column Connection with Weld Defects, *Journal of Structural and Construction Engineering (Transactions of AIJ)*, Volume 67, Issue 556, Pages 145-150.
- [13] Irwin G (1957), Analysis of stresses and strains near the end of a crack traversing a plate, *Journal of Applied Mechanics* 24, 361–364.
- [14] Newman J C Jr. and Raju I S (1984), *NASA Technical Memorandum*, 85793.



17th World Conference on Earthquake Engineering, 17WCEE

Sendai, Japan - September 13th to 18th 2020

- [15] American Petroleum Institute (2016), *API 579-1 ASME FFS-1*, Fitness-For-Service
- [16] Ritchie R O, Knott J F, Rice J R (1973), On the relationship between critical tensile stress and fracture toughness in mild steel, *Journal of the Mechanics and Physics of Solids*, Volume 21, Issue 6, Pages 395-410
- [17] Pineau A (1981), *Advanced in Frac. Res.*, 5th I.C.F., D. Francois, Eds., 2, 553.